Journal of
Materials Chemistry B

Accepted Manuscript

This article can be cited before page numbers have been issued, to do this please use: H. Liu, T. Liu, J. Li, Y. Zhang, J. Li, J. Song, J. Qu and W. (. Wong, *J. Mater. Chem. B*, 2018, DOI: 10.1039/C8TB01743C.

ROYAL SOCIETY OF CHEMISTRY

rsc.li/materials-b

View Article Online
DOI: 10.1039/C8TB01743C

Graphical Abstract

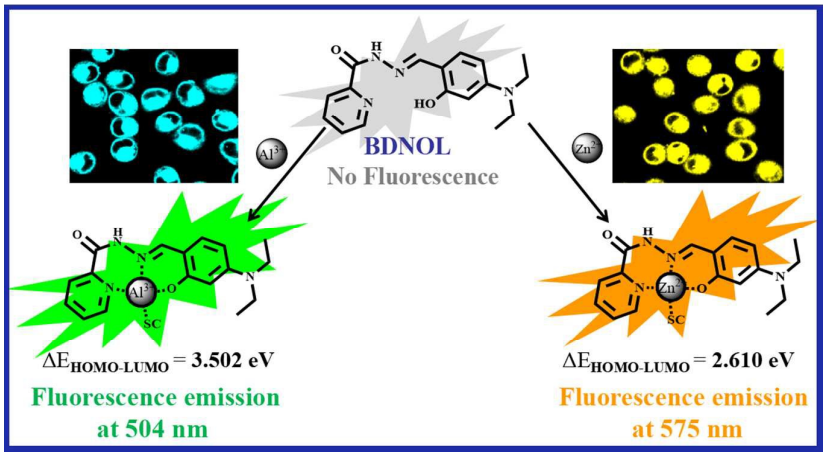

The chemosensor BDNOL can selectively recognize Al^{3+} and Zn^{2+} with significant fluorescence enhancement at 504 nm and 575 nm.

View Article Online
DOI: 10.1039/C8TB01743C

Journal Name

ARTICLE

A simple Schiff base as dual-responsive fluorescent sensor for bioimaging recognition of Zn^{2+} and Al^{3+} in living cells

Received 00th January 20xx,
Accepted 00th January 20xx

DOI: 10.1039/x0xx00000x

www.rsc.org/

Haiyang Liu[a,b], Tianqi Liu[c], Jia Li[a], Youming Zhang[a,b], Jiahua Li[b], Jun Song[a*], Junle Qu[a*], Wai-Yeung Wong[a,b*]

A simple Schiff base fluorescent sensor (BDNOL) was synthesized from the reaction of picolinohydrazide and 4-(diethylamino)salicylaldehyde, and developed for selective detection of Al^{3+} and Zn^{2+}. This non-fluorescent sensor displayed obvious fluorescence enhancement after binding to Al^{3+}/Zn^{2+} ions with high sensitivity and selectivity, accompanied by obvious fluorescence emission enhancement (504 nm emission for Al^{3+} and 575 nm for Zn^{2+}). The detection limits were found to be 8.30×10^{-8} M for Al^{3+} and 1.24×10^{-7} M for Zn^{2+}, respectively. The binding mechanisms between BDNOL and Al^{3+}/Zn^{2+} ions were supported by ^{1}H NMR, HR-MS analysis, and density functional theory (DFT) study. The sensing behavior was also studied with molecular logic functions of OR, AND, and NOT gates. Furthermore, the fluorescent sensor was successfully used to recognize Al^{3+} and Zn^{2+} in living cells, suggesting that this simple biosensor has a great potential in the application of biological imaging.

Introduction

As an indispensable transition metal for life, Zn^{2+} plays significant roles in many physiological processes, and its metabolism disorder is linked with neurodegenerative diseases, such as Alzheimer's, Parkinson's and epilepsy disease.[1-3] It has been found that Al^{3+} is not necessary for the human body, although it ranks as the most prevalent metal element in the earth's crust.[4,5] People can easily get Al^{3+} intake via daily diet, because the aluminum products are widely used in our daily life [6]. However, excessive intake of Al^{3+} can also cause serious damage to the central nervous system for human and increase the risk of Alzheimer's disease, Parkinson's disease and amyotrophic lateral sclerosis (ALS).[5,7,8] Therefore, it is of considerable importance and highly desirable to design and develop efficient biosensors to monitor Zn^{2+} and Al^{3+} in biological system.

Fluorescence detection methods have attracted enormous attention for qualitative and quantitative detection of relevant metal ions and anions of organism, owing to their immediate response, high sensitivity, easy visualization, real-time analysis, and non-destructive nature in the living system.[9-20] Until recently, plenty of fluorescent probes have been developed for monitoring the metal ions of human, such as Fe^{3+}, Zn^{2+}, Cu^{2+}, Al^{3+}, Cr^{3+}, Cd^{2+}, Hg^{2+}, etc.[4,6,19-30] Many of these chemosensors have excellent performance in the process of sensing one specific target metal ion, but they can not proceed in one-to-multi sensing. Compared to those one-to-one type sensors, to develop simple, efficient and functionalized fluorescent sensor with both biological activity and multi-analyte response is challenging from the viewpoints of economic value and practical applications.

In recent years, several one-to-multi type fluorescent sensors developed for different metal ions have been reported.[24,30-37] Kim et al. developed a rhodamine-based and dual-responsive sensor to selectively recognize Al^{3+} and Cu^{2+} by using different signaling channels, UV absorption and fluorescence.[30] Hu et al. designed a rhodamine-phenylurea conjugate derivative to selectively detect Pb^{2+} in aceyonitrile, and Hg^{2+} in aqueous media, respectively.[31] Emrullahoğlu et al. developed a rhodamine-BODIPY derivative for selective recognition of Hg^{2+} and Au^{3+} with different excitation wavelength.[32] Liu et al. designed and synthesized a quinoline-based fluorescent sensor, which can be employed to selectively recognize Cd^{2+} and Zn^{2+} via two different binding mechanisms.[34] However, there are few dual-responsive chemosensors reported for selective recognition of Al^{3+} and Zn^{2+} in the biosystem, while monitoring these two metals in organism is of great importance due to their roles to human health and disease.

Salicylaldehyde Schiff base derivatives have received wide attention in the field of sensing metal ions, because these chemosensors contain nitrogen-oxygen-rich coordination

[a] Key Laboratory of Optoelectronic Devices and Systems of Ministry of Education and Guangdong Province, College of Optoelectronic Engineering, Shenzhen University, Shenzhen 518060, PR China Email: songjun@szu.edu.cn; jlqu@szu.edu.cn
[b] Department of Applied Biology and Chemical Technology, The Hong Kong Polytechnic University, Hung Hom, Hong Kong, PR China Email: wai-yeung.wong@polyu.edu.hk
[c] Department of Chemistry, KTH Royal Institute of Technology, 10044 Stockholm, Sweden

Electronic Supplementary Information (ESI) available: [details of any supplementary information available should be included here]. See DOI: 10.1039/x0xx00000x

View Article Online
DOI: 10.1039/C8TB01743C

circumstance which can coordinate with metal ions, leading to interesting photophysical property changes.[22,25,28-30,38] In the structure of salicylaldehyde Schiff base, the -OH group can form a six-membered transition state with the adjoining imine bond, leading to excited state intramolecular proton transfer (ESIPT).[38,39] After chelating with metal ions, the ESIPT process is restrained, and meanwhile the -CH=N- isomerization is also inhibited, both of which could cause optical signal changes of the salicylaldehyde Schiff base fluorescent sensor.[33,38,39] With this in mind, we synthesized and developed a simple Schiff base fluorescent sensor (BDNOL), derived from the reaction of picolinohydrazide and 4-(diethylamino)salicylaldehyde, which displayed favorable selectivity for Zn^{2+} and Al^{3+} over other competitive metal ions. In the sensing process, the O atom of phenolic hydroxyl group, and the N atoms of imine bond and pyridine unit coordinate to the respective central metal, accompanied by an obvious fluorescence emission enhancement in each case (504 nm emission for Al^{3+} and 575 nm for Zn^{2+} respectively). The density functional theory (DFT) calculations were also performed to investigate the emission difference between Al^{3+} and Zn^{2+}. Moreover, further application of BDNOL in fluorescence tracing of Zn^{2+} and Al^{3+} in living cells was studied, suggesting that this Schiff base compound can be used as a potential biosensor for Zn^{2+} and Al^{3+} in living system.

Experimental section

Synthesis of BDSBL

Picolinohydrazide was prepared by the reaction of methyl pyridine-2-carboxylate and hydrazinium hydrate in the refluxing methanol via a reported method (^{1}H NMR and ^{13}C NMR spectra are shown in Fig. S1 and S2).[40] Into a 50 mL two-necked flask, picolinohydrazide (0.411 g, 0.003 mol) and 4-(diethylamino)salicylaldehyde (0.580 g, 0.003 mol) were added and dissolved in 15 mL anhydrous ethanol. The mixture solution was stirred at 60 °C for 5 h, and then a yellow precipitate was obtained. The solid residue was collected by filtration and washed with cold ethanol (15 mL). After 6 hours with vacuum drying at 50 °C, a pale yellow powder was obtained, 0.693 g, yield: 74%. ^{1}H NMR (400 MHz, DMSO-d_6) d (ppm): 12.22 (s, 1H), 11.59 (s, 1H), 8.71 (d, J = 7.6 Hz, 1H), 8.58 (d, 1H), 8.08 (m, 2H), 7.66 (t, J = 3.8 Hz, 1H), 7.13 (d, J = 8.4Hz, 1H), 6.27 (d, J = 8.4 Hz, 1H), 6.13 (s, 1H), 3.36 (q, J = 7.0 Hz, 4H), 1.11 (t, J = 7.0 Hz, 6H). ^{13}C NMR (100 MHz, DMSO-d_6) d (ppm): 160.40, 160.15, 151.93, 150.71, 149.98, 149.02, 138.51, 132.41, 127.39, 123.07, 106.94, 104.17, 98.00, 44.31, 13.05. HRMS calcd for $C_{17}H_{21}N_4O_2$ [BDNOL+H]$^+$: 313.1665, found: 313.1659.

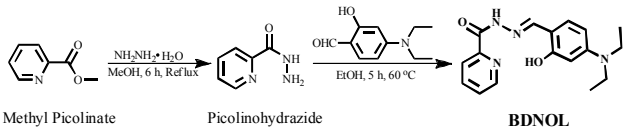

Scheme 1. The synthetic route of BDNOL

Fluorescence and UV-vis studies

Stock solutions of metal chlorides (0.001 M) and sodium fluoride (0.001 M) were prepared in 20 mM HEPES buffer (pH 7.2), and BDNOL solution was prepared in DMSO (0.001 M). The concentration of BDNOL for fluorescence and UV-vis measurements was diluted to 10 μM in CH_3OH/HEPES buffer (1/4, v/v, pH 7.2). All spectral data were recorded in 5 min after the addition of cations and anions at room temperature.

DFT calculations

Geometry optimization of BDNOL and [BDNOL-Zn^{2+}]/[BDNOL-Al^{3+}] were performed by the DFT/B3LYP method using Gaussian 09 software.[41] The 6-311G basis set was used for C, H, N, O and the LanL2DZ basis set was used for the effective potential (ECP) set for Zn^{2+} and Al^{3+}. The geometries of all structures were fully optimized and normal mode analysis was used to confirm the nature of the stationary points and evaluate the thermochemical properties.

Cellular imaging

HeLa cells were cultured in RPMI-1640 medium with 10% fetal bovine serum (FBS) at 37 °C under a humidified atmosphere of 5% CO_2. The cells were incubated with BDNOL for 6 h and washed with PBS buffer for three times. Then the cells were incubated with Zn^{2+} or Al^{3+} (50 μM) for another 2 h. Finally, the seeded cells were imaged using a laser scanning confocal fluorescence microscope.

The cell cytotoxicity of BDNOL was measured by a standard MTT assay.[42] HeLa cells were seeded in 96-well plates with different concentrations of BDNOL (ranged from 2 to 50 μM). After incubation with BDNOL for 12 h, MTT (10 μM) solution was added into each well of a 96-well plate and incubated for another 4 h. Then the medium was removed and replaced with 100 μL DMSO in each well. Finally, the optical density of each well was measured with a microplate reader at 490 nm. The cell viability was calculated from the optical density ratio of the treatment sample to the control (The cytotoxicity measurements were repeated for three times).

Results and discussion

BDNOL was facilely synthesized by the reaction of picolinohydrazide and 4-(diethylamino)salicylaldehyde in the refluxing methanol as shown in Scheme 1, and the structure was then confirmed by ^{1}H NMR (Fig. S3), ^{13}C NMR (Fig.S4), and HRMS measurements (Fig. S5).

Selectivity of BDNOL for Al^{3+} and Zn^{2+}

The UV-vis and fluorescent spectra of BDNOL were tested in CH_3OH/HEPES buffer (1/4, v/v, pH 7.2) in the presence of various metal ions (Na^+, K^+, Mg^{2+}, Ca^{2+}, Cu^{2+}, Ni^{2+}, Mn^{2+}, Co^{2+}, Fe^{2+}, Fe^{3+}, Cr^{3+}, Ag^+, Cd^{2+}, Hg^{2+}, Pb^{2+}, Al^{3+} and Zn^{2+}). As shown in Fig. S6, broad absorption around 375 nm was

View Article Online
DOI: 10.1039/C8TB01743C

observed for BDNOL, while there is almost no significant change in the absorption spectrum within 300-550 nm among

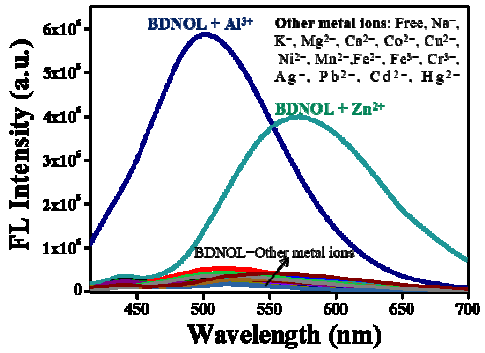

Fig. 1. Fluorescence emission spectra obtained for BDNOL (10 μM) after the addition of 5.0 equiv. of various metal ions in CH_3OH/HEPES buffer (1/4, v/v, pH 7.2) (λ_{ex}: 390 nm).

most of the added metal ions (5.0 equiv.) except Al^{3+} and Zn^{2+}. Upon the addition of Al^{3+} and Zn^{2+}, the absorption band centered at 375 nm exhibited a large red-shift to 405 nm and dramatic absorption enhancement for Al^{3+}, and a larger red-shift to 434 nm and absorption enhancement for Zn^{2+}, accompanied by an obvious color change from colorless to light brown and light yellow respectively. In the fluorescence test, free BDNOL exhibited scarcely fluorescence emission. Upon addition of the metal ions, only Al^{3+} and Zn^{2+} induced apparent fluorescence changes. On the other hand, other metal ions had almost no effects on the fluorescence emission. As shown in Fig. 1, Al^{3+} and Zn^{2+} ions can be easily distinguished from the different fluorescence emission characteristics, because significant fluorescence enhancements centered at 504 nm and 575 nm were obtained for Al^{3+} and Zn^{2+}, respectively.

The BDNOL fluorescence enhancement phenomenon after encountering Al^{3+} or Zn^{2+} can be attributed to the formation of stable complexes between BDNOL and Al^{3+}/Zn^{2+}, leading to the chelation-enhanced fluorescence (CHEF) effect via the phenolic hydroxyl O, the imine bond N, and the pyridine N chelating the central metal.[25,40,43-47] More importantly, after BDNOL binds to Al^{3+}/Zn^{2+}, the -CH=N- isomerization is inhibited, and meanwhile the coordination of N,N,O towards Al^{3+}/Zn^{2+} ions also prevents the ESIPT process, both of which are conducive to fluorescence emission enhancement of BDNOL.[38,39,45,48]

The specificity of BDNOL's fluorescence responses towards Al^{3+} and Zn^{2+} ions was examined by competitive experiments. As shown in Fig. 2a, no significant interference was observed in BDNOL-Al^{3+} solution in the presence of other metal ions. Then, BDNOL was treated with Zn^{2+} in the presence of other competitive metal ions (10 equiv.). The solution of BDNOL-Zn^{2+} showed almost no fluorescence variation against other metal ions except Al^{3+} (Fig. 2b). As seen in Fig. 2b, the introduction of Al^{3+} into the system of BDNOL-Zn^{2+} can cause a blue-shift of the fluorescence emission from 575 nm to 504 nm (the original fluorescence peak of BDNOL-Al^{3+}), suggesting that the receptor BDNOL has a stronger binding affinity towards Al^{3+} than Zn^{2+}. It is an important question to be solved on how to determine whether Zn^{2+} exists in the BDNOL-Al^{3+} solution.

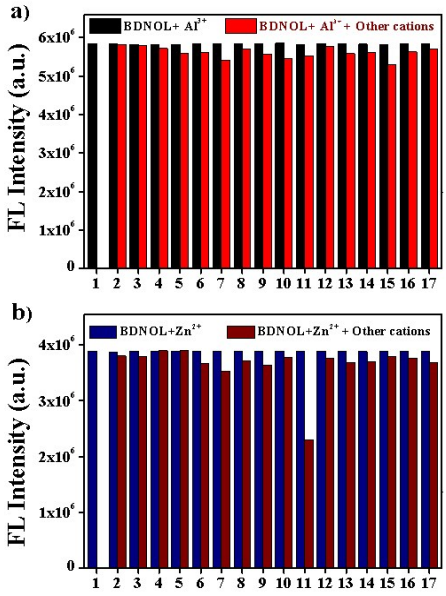

Fig. 2. (a) The fluorescence intensity at 504 nm of BDNOL (10 μM) with 5.0 equiv. of Al^{3+}, and then added 10.0 equiv. of various metal ions, and (b) the fluorescence intensity at 575 nm of BDNOL (10 μM) with 5.0 equiv. of Zn^{2+}, and then added 10.0 equiv. of various metal ions in CH_3OH/HEPES buffer (1/4, v/v, pH 7.2). 1, Al^{3+} (a)/ Zn^{2+} (b);2, Na^+; 3, K^+; 4, Mg^{2+}; 5, Ca^{2+}; 6, Mn^{2+}; 7, Cu^{2+}; 8, Co^{2+}; 9, Ni^{2+}; 10, Fe^{2+}; 11, Zn^{2+}; 12, Fe^{3+}; 13, Cr^{3+}; 14, Cd^{2+}; 15, Pb^{2+}; 16, Hg^{2+}; 17, Ag^+. (λ_{ex}: 390 nm).

Of particular importance is that fluoride anion (F^-) can be used as a masking agent towards Al^{3+} by the formation of stable aluminum fluoride complexes (AlF_x).[49,50] If both of Zn^{2+} and Al^{3+} exist in a solution simultaneously, the introduction of F^- can cause AlF_x species to be generated, releasing free BDNOL which can subsequently chelate Zn^{2+} accompanied by a obvious fluorescence emission red-shift to 575 nm from 504 nm (Fig. 3). Through the displacement strategy, it can be used to determine the existence of Zn^{2+} in the Al^{3+}-Zn^{2+} solution. The above results indicate that the simple Schiff base can act as a potential fluorescent sensor for the selective detection of Al^{3+} and Zn^{2+}.

View Article Online
DOI: 10.1039/C8TB01743C

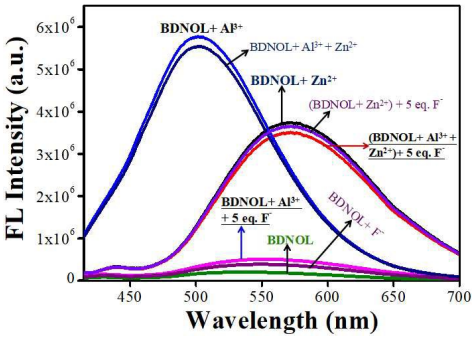

Fig. 3. Fluorescence emission spectra of 10 μM of BDNOL, BDNOL-Al^{3+}, BDNOL-Al^{3+}, and BDNOL-Al^{3+}&Zn^{2+} after addition of F^- in CH_3OH/HEPES buffer (1/4, v/v, pH 7.2) (λ_{ex}: 390 nm).

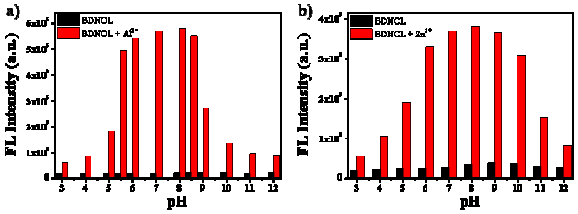

Fig. 4. (a) Fluorescence intensity at 504 nm and 575 nm recorded for BDNOL (10 μM) at various pH values in the absence and presence of 5 equiv. of (a) Al^{3+}, and (b) Zn^{2+}, respectively.

Effect of pH and response time

The pH variation effects on fluorescence intensity of BDNOL and BDNOL-Al^{3+}/BDNOL-Zn^{2+} are depicted in Fig. 4. There is no obvious fluorescence change of BDNOL at a variable pH range from 3.0 to 12.0. When Al^{3+} is introduced, a significant fluorescence intensity enhancement of BDNOL-Al^{3+} is observed from pH 5.5 to pH 8.5 (Fig. 4a). Little fluorescence change is found in the pH range from pH 3.0 to pH 5.0 and from pH 9.0 to pH 12.0. The acidic conditions can induce dissociation of the BDNOL-Al^{3+} complex because of the protonation of BDNOL,[51] and the higher pH conditions can provide sufficient hydroxyl ions to extract metal ion from BDNOL-Al^{3+} complex to form the hydrolyzed complexes.[50,52] A similar phenomenon was also found in BDNOL-Zn^{2+} system, and an increase of fluorescence intensity caused by the addition of Zn^{2+} was observed in a range of pH 6.0~10.0 (Fig. 4b). The pH effect study clearly indicated that the best fluorescence behavior of BDNOL towards both of Al^{3+} and Zn^{2+} are under physiological window at pH=7.4, which is conducive to using the fluorescent sensors in the biological systems.[53]

The time dependent fluorescence intensity of BDNOL in presence of Al^{3+} and Zn^{2+} ions was also studied, respectively. As seen in Fig. S7, the fluorescence intensity of BDNOL (504 nm) basically reached the maximum in one minute after addition of Al^{3+} and remained almost unchanged over a period of 30 min. In the process of sensing Zn^{2+}, a faster recognition behavior can be observed and the maximum fluorescence intensity (575 nm) remained almost unchanged (~30 min) after about 40 seconds. The instant fluorescence response and fluorescence stability suggests that BDNOL has the potential of practical application.

Fluorescence titration study

In order to estimate the sensing capability of BDNOL toward Al^{3+} and Zn^{2+}, the detail fluorescence titration analysis was further investigated. As shown in Fig. 5, with gradual addition of Al^{3+} and Zn^{2+} (0-5.0 equiv.), the fluorescence emission of BDNOL was significantly enhanced at 504 nm and 575 nm, respectively. The fluorescence spectra were recorded upon the addition of different concentrations of Al^{3+} and Zn^{2+} from 0.2 to 50 μM (Fig. 5a and Fig. 5b). BDNOL showed nice linear relationships (R^2 = 0.995 for Al^{3+} and R^2 = 0.989 for Zn^{2+}, respectively) between the fluorescence intensity and Al^{3+}/Zn^{2+}

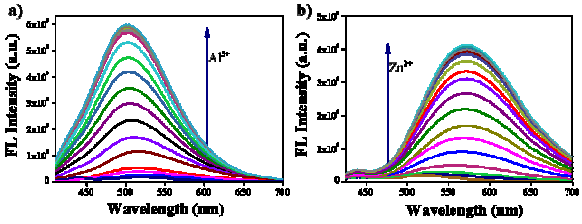

Fig. 5. Fluorescence emission spectra recorded for BDNOL (10 μM) upon gradual addition 0-50 μM of (a) Al^{3+} and (b) Zn^{2+} in CH_3OH/HEPES buffer (1/4, v/v) (λ_{ex}: 390 nm).

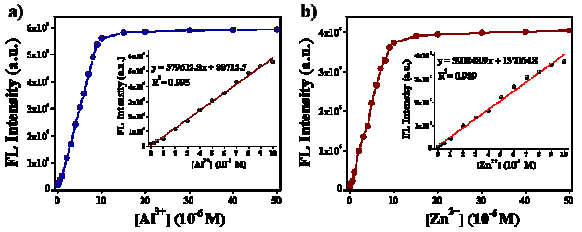

Fig. 6. Calibration curve obtained for the fluorescence intensity at the emission peak of BDNOL (10 μM) versus the concentration of (a) Al^{3+} and (b) Zn^{2+} (0-50 μM), and the inset shows the linear range (0-10 μM) of the curve.

concentrations (0.2~10 μM) (Fig. 6a and Fig. 6b). The detection limits were determined as 8.30×10^{-8} M for Al^{3+} and 1.24×10^{-7} M for Zn^{2+} on the basis of the IUPAC recommendation of $3\sigma/S$,[54] where σ is the standard deviation of the control sample and S is the slope of the calibration curve. The obtained detection limits are much lower than the enforceable drinking water standard for Al^{3+} (7.4 μM) and Zn^{2+} (45.9 μM) developed by the World Health Organization (WHO).[55]

Considering the potential use of BDNOL for practical samples, the presence of Al^{3+}/Zn^{2+} ions in tap-water was tested to evaluate its practical feasibility. As seen in Fig. S8, the fluorescence intensity of emission peak increased gradually upon addition of Al^{3+} and Zn^{2+}, respectively (2.0-9.0 μM), and the total Al^{3+}/Zn^{2+} concentrations in practical samples were quantitatively derived from fitted linear calibration curves (each

View Article Online
DOI: 10.1039/C8TB01743C

practical sample had four replicates). The recovery and relative standard deviation (RSD) of BDNOL were 97.0-100.3% and 1.32-3.82% for Al^{3+}, and 101.5-102.2% and 0.84-4.64% for Zn^{2+}, respectively (Table S1). The fluorescence titration analysis and tap-water verification test indicate that the Schiff base sensor can be used to quantitatively detect Al^{3+}/Zn^{2+} in practical water samples.

Binding mechanism study

On the basis of the Job's plot analyses, the binding stoichiometries of the interaction between BDNOL and Al^{3+}, and BDNOL and Zn^{2+} were both calculated as 1:1 (Fig. S9). The mass spectrometry is another direct evidence to investigate the binding ratio between BDNOL and the central metal. As shown in Fig. S10, all these ESI-mass data clearly indicated the formation of 1:1 complex between BDNOL-Al^{3+}/Zn^{2+}. Based on the binding stoichiometry analysis and Benesi-Hildebrand equation,[56,57] the association constants (K_a) were determined to be 1.3×10^6 M^{-1} for BDNOL-Al^{3+}, and 7.9×10^4 M^{-1} for BDNOL-Zn^{2+} from the fluorescence titration fitting curves (Fig. 6). Compared with the BDNOL-Zn^{2+} complex, the generation of more stable aluminum complex is due to the higher binding affinity towards the Schiff base BDNOL which provided a hard base environment.[58]

In order to understand the binding mechanism of BDNOL with Al^{3+}/Zn^{2+}, the ^1H NMR test of BDNOL has been conducted by concomitant additon of 1.0 equiv. of Al^{3+}/Zn^{2+} ions. As seen in Fig. S11 and S12, after addition of these metal ions, the proton H_f of phenol hydroxyl group at 11.59 ppm almost disappeared, and the proton H_g of imine group shifted downfield ($\Delta\delta$ was up to 0.13 ppm for Al^{3+} and 0.19 ppm for Zn^{2+}, respectively). The protons H_i, H_j, H_k and H_l of pyridine unit also shifted downfield ($\Delta\delta$ was up to 0.22 ppm, 0.22 ppm, 0.25 ppm and 0.06 ppm for Al^{3+} addition, and up to 0.24 ppm, 0.24 ppm, 0.27 ppm and 0.20 ppm for Zn^{2+} addition, respectively). The ^1H NMR results suggested that the O atom of hydroxyl unit, the N atoms of imine group and pyridine unit might coordinate to the central Al(III)/Zn(II). The binding behavior of BDNOL toward Al^{3+}/Zn^{2+} was consistent with the previous reports.[59,60]

To obtain a better understanding of the binding mode of BDNOL and Al^{3+}/Zn^{2+}, and why the introduction of these two cations could cause different fluorescence emission, the DFT calculations with B3LYP method were performed. The calculated minimal structures of BDNOL and BDNOL-Al^{3+}/Zn^{2+} complexes with the key structural properties are shown in Fig. 7. The distances of Al^{3+} from the pyridine N, imine N and hydroxyl O are 1.98, 1.93 and 1.77 Å, and Zn^{2+} from the pyridine N, imine N and hydroxyl O are 2.07, 2.02 and 1.92 Å, respectively. These spatial data indicate that these optimized structure could provide adequate space to accommodate Al^{3+}/Zn^{2+} ions. Time-dependent DFT (TD-DFT) calculations were also performed at the optimized geometries.

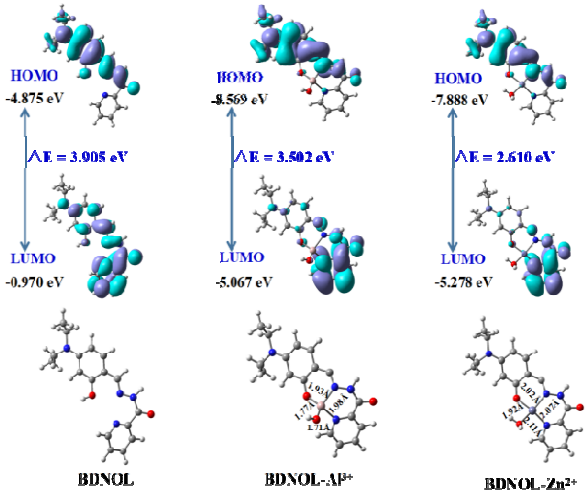

Fig. 7. Frontier molecular orbital profiles of BDNOL, BDNOL–Al^{3+} and BDNOL–Zn^{2+} based on DFT calculations.

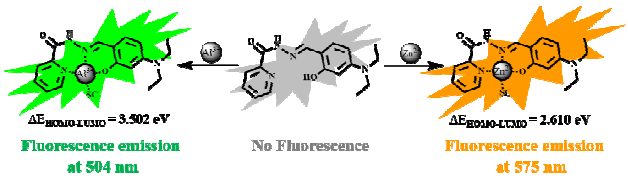

Scheme 2. Proposed binding modes of BDNOL for the recognition of Al^{3+} and Zn^{2+} (SC: Solvent circumstances).

The energy band gap ΔE between the HOMO and LUMO of BDNOL, BDNOL–Al^{3+} and BDNOL–Zn^{2+} were 3.905 eV, 3.502 eV and 2.610 eV, respectively, which indicate that the interaction of Al^{3+}/Zn^{2+} and BDNOL resulted in the changes in electronic and photophysical properties of this Schiff base sensor. In addition, the theoretical energy gap of BDNOL–Zn^{2+} (2.610 eV) is narrower than that of BDNOL–Al^{3+} (3.502 eV), and the actual fluorescence emission peak of BDNOL–Zn^{2+} shows a larger red-shift to 575 nm compared to the emission peak of BDNOL–Al^{3+} at 504 nm, which is also consistent with the principles of quantum chemistry.[61] According to the Job's plot, ESI-mass analysis, ^1H NMR study and DFT calculations, the binding modes of BDNOL-Al(III)/Zn(II) are proposed in Scheme 2.

Logic gate behavior of BDNOL

The logic gate analysis is an important functionalization and application of molecular sensor.[62-64] The fluorimetric sensing processes of BDNOL towards Al^{3+} and Zn^{2+} were also studied in a molecular logic circuit, in which these two metal ions and F^- were used as three inputs, and the obtained fluorescence intensity signals of 504 nm and 575 nm served as two outputs (Fig. 8a and 8b). As shown in Fig. 8c, in the "Output 504 nm" logic analysis, either of the inputs "Al^{3+}" and "Al^{3+} AND Zn^{2+}" is assigned with "1" (504 nm fluorescence emission "turn-on"). In the "Output 575 nm" logic analysis, each of the inputs "Zn^{2+}", "Zn^{2+} AND F^-" and "Zn^{2+} AND Al^{3+} AND F^-" is assigned with "1" (575 nm fluorescence emission "turn-on").

View Article Online
DOI: 10.1039/C8TB01743C

While all the other inputs, includig "F^- " and "Al^{3+} AND F^-", are assigned with "0" (no fluorescence emission "turn-on"). This logic gate study showed that this single fluorescence sensor could perform arithmetic operations, which is like a signal transmission computer.

Cytotoxicity and cell imaging

The cytotoxicity of BDNOL was also performed by a MTT assay before its bioimaging application (Fig. S13). The following MTT study shows that BDNOL (20 μM) has low cytotoxicity towards cells, indicating that this simple fluorescent chemosensor has a good potential for biological applications. In the experiment of cell imaging, the HeLa cells were incubated with BDNOL (20 μM) for 4 h and then treated with metal ions (50 μM of Al^{3+} or Zn^{2+} ions) for another 2 h. The cells incubated with the chemosensor only exhibited negligible fluorescence (Fig. 9a), while an obvious green fluorescence image was observed after the addition of Al^{3+} ions (Fig. 9b), and a new orange fluorescence image could be observed for Zn^{2+} ions addition (Fig. 9c), indicating that BDNOL has a very good performance for Al^{3+} and Zn^{2+} ions imaging in Hela cells. The cell imaging results suggest that this Schiff base sensor can be employed for fluorescence imaging of Al^{3+} and Zn^{2+} ions selectively in living cells.

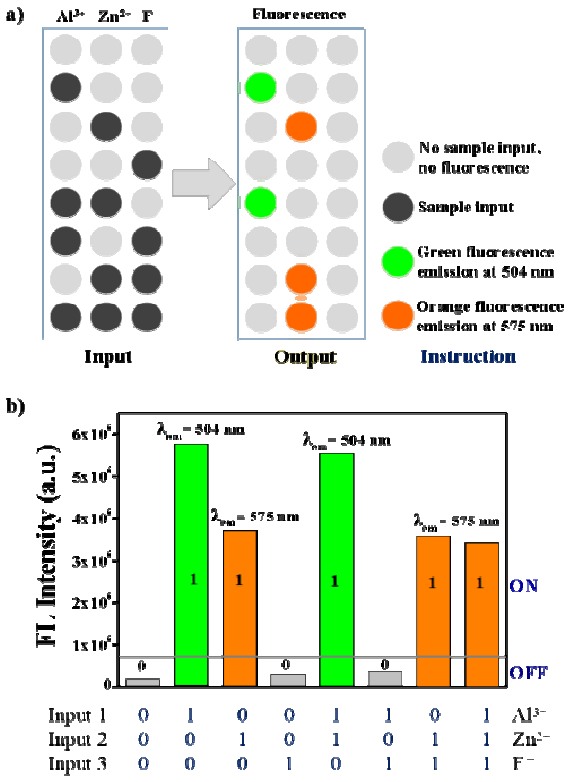

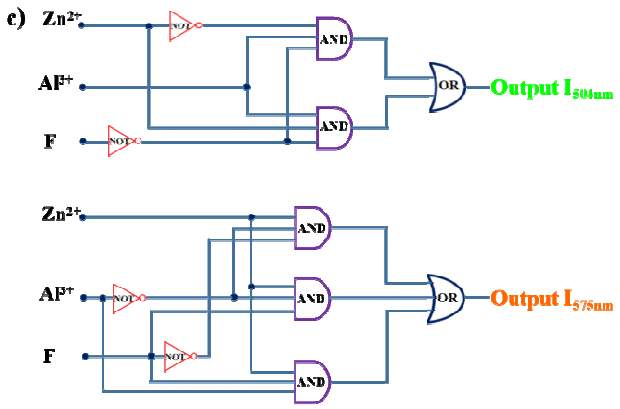

Fig. 8. The corresponding visualization figure, (b) the fluorescence emission output bar diagram, and (c) the molecular logic circuit with three inputs (Zn^{2+}, Al^{3+} and F^-) and two outputs (fluorescence emission at 504 nm and 575 nm.

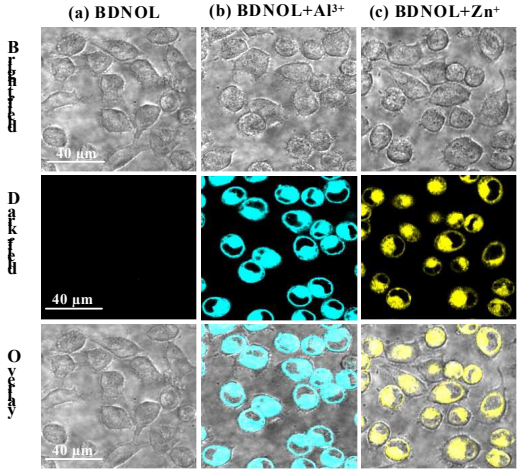

Fig. 9. Fluorescence microscopy images of HeLa cells. (a) Cells were incubated with 20 μM BDNOL for 4 h, (b) Cells were incubated with 10 μM BDNOL for 4 h, and further incubated with 50 μM Al^{3+} for 2 h, (c) Cells were incubated with 10 μM BDNOL for 4 h, and further incubated with 50 μM Zn^{2+} for 2 h.

Conclusions

In summary, a simple Schiff base fluorescent sensor BDNOL was developed for the selective recognition of Al^{3+} and Zn^{2+} ions. This non-fluorescent sensor can be used to sensitively detect Al^{3+} and Zn^{2+}, leading to obvious fluorescence enhancement at 504 nm and 575 nm, respectively. The fluorescence enhancement mechanism of sensing Al^{3+} and Zn^{2+} is based on the CHEF effect, the -CH=N- isomerization, and the inhibition of ESIPT process. The recognition mechanism has also been investigated by ^{1}H NMR, ESI-mass analysis and DFT calculations in details. In addition, BDNOL was used for the

View Article Online
DOI: 10.1039/C8TB01743C

fluorescence imaging of Al^{3+} and Zn^{2+} selectively in living cells, indicating that this simple biosensor can be potentially applied for the recognition of Al^{3+}/Zn^{2+} in biological systems.

Conflicts of interest

There are no conflicts to declare.

Acknowledgements

This work was supported by the National Basic Research Program of China (2015CB352005); the National Natural Science Foundation of China (61775145, 61605124, 31771584, 61525503, 61620106016, 81727804, 61605130, 51602201); Guangdong Natural Science Foundation Innovation Team (2014A030312008); and Shenzhen Basic Research Project (JCYJ20170412110212234, JCYJ20160308093035903, JCYJ20150930104948169, JCYJ20160328144746940, GJHZ20160226202139185), the Hong Kong Polytechnic University (1-ZE1C). T.L. is supported by the China Scholarship Council and Ms. Clarea Au (847S for the Endowed Professorship).

Notes and references

1 A. I. Bush, W. H. Pettingell, G. Multhaup, M. Paradis, J. P. Vonsattel, J. F. Gusella, K. Beyreuther, C. L. Masters, R. E. Tanzi, *Science*, 1994, **265**, 1464–1467.
2 C. J. Frederickson, J. Y. Koh, A. I. Bush, *Nat. Rev. Neurosci.*, 2005, **6**, 449–462.
3 J. M. Goldberg, F. Wang, C. D. Sessler, N. W. Vogler, D. Y. Zhang, W. H. Loucks, T. Tzounopoulos, S. J. Lippard, *J. Am. Chem. Soc.*, 2018, **140**, 2020–2023.
4 S. C. Bondy, Toxicology, 2014, **315**, 1–7.
5 C. Exley, *Expert Rev. Neurother.*, 2014, **14**, 589–591.
6 Y.i Chen, T. Wei, Z. Zhang, T. Chen, J. Li, J. Qiang, J. Lv, F. Wang, X. Q. Chen, *Ind. Eng. Chem. Res.*, 2017, **56**, 12267–12275.
7 Z. Wang, X. Wei, J. Yang, J. Suo, J. Chen, X. Liu , X. L. Zhao, *Neurosci. Lett.*, 2016, **610**, 200–206.
8 R. Kandimalla, J. Vallamkondu, E. B Corgiat, K. D. Gill1, *Brain Pathol.*, 2016, **26**, 139–154.
9 P. S. Zhang, H. Wang, D. Zhang, X. Y. Zeng, R. J. Zeng, L. H. Xiao, H. W. Tao, Y. F. Long, P. G. Yi, J. Chen, *Sens. Actuators B*, 2018, **255**, 2223–2231.
10 L. J. Hou, X. Y. Kong, Y. S. Wang, J. B. Chao, C. Z. Li, C. Dong, Y. Wang, S. M. Shuang, *J. Mater. Chem. B*, 2017, **5**, 8957–8966.
11 Y. Q. Tang, J. G. Sun, B. Z. Yin, *Anal. Chim. Acta*, 2016, **942**, 104–111.
12 P. S. Zhang, H. Wang, Y. X. Hong, M. L. Yu, R. J. Zeng, Y. F. Long, J. Chen, *Biosens. Bioelectron.*, 2018, **99**, 318–324.
13 M. G. Ren, K. Zhou, L. W. He, W. Y. Lin, *J. Mater. Chem. B*, 2018, **6**, 1716–1733.
14 H. Wang, P. S. Zhang, Y. X. Hong, B. Zhao, P. G. Yi, J. Chen, *Polym. Chem.*, 2017, **8**, 5795–5802.
15 D. Wu, A. C. Sedgwick, T. Gunnlaugsson, E. U. Akkaya, J. Yoon, T. D. James, *Chem. Soc. Rev.*, 2017, **46**, 7105–7123.
16 X. Kong, F. Su, L. Zhang, J. Yaron, F. Lee, Z. Shi, Y. Tian, D. R. Meldrum, *Angew. Chem. Int. Ed.*, 2015, **54**, 12053–12057.
17 J. Yin, Y. Hua, J. Yoon, *Chem. Soc. Rev.*, 2015, **44**, 4619–4644.
18 L. E. Jennings, N. J. Long, *Chem. Commun.*, 2009, 3511–3524.
19 K. P. Carter, A. M. Young, A. E. Palmer, *Chem. Rev.*, 2014, **114**, 4564–4601.
20 D. Wua, L. Chen, W. Lee, G. Ko, J. Yin, J. Yoon, *Coord. Chem. Rev.*, 2018, 354, 74–97.
21 L. Peng, Z. Zhou, X. Wang, R. Wei, K. Li, Y. Xiang, A. J. Tong, *Anal. Chim. Acta*, 2014, **829**, 54–59.
22 S. Das, A. Sarkar, A. Rakshit, A. Datta, *Inorg. Chem.*, 2018, **57**, 5273–5281.
23 L. Hou, X. Kong, Y. Wang, J. Chao, C. Li, C. Dong, Y. Wang, S. Shuang, *J. Mater. Chem. B*, 2017, **5**, 8957–8966.
24 J. Dong, J. Hu, H. Baigude, H. Zhang, *Dalton Trans.*, 2018, **47**, 314–322.
25 Y. Jeong, J. Yoon, *Inorg. Chim. Acta*, 2012, **381**, 2–14.
26 X. D. Yang, X. L. Chen, X. D. Lu, C. G. Yan, Y. K. Xu, X. D. Hang, J. Q. Qu, R. Y. Liu, *J. Mater. Chem. C*, 2016, **4**, 383–390.
27 Y. Zhang, X. Guo, M. Zheng, R. Yang, H. Yang, L. Jia, M. Yang, *Org. Biomol. Chem.*, 2017, **15**, 2211–2216.
28 S. Goswami, A. K. Das, A. K. Maity, A. Manna, K. Aich, S. Maity, P. Saha, T. K. Mandal, *Dalton Trans.*, 2014, **43**, 231–239.
29 T. W. Price, G. Firth, C. J. Eling, M. Kinnon, N. J. Long, J. Sturgea, G. J. Stasiuk, *Chem. Commun.*, 2018, **54**, 3227–3230.
30 H.-S. Kim, S. Angupillai, Y. Son, *Sens. Actuators B*, 2016, **222**, 447–458.
31 Z.-Q. Hu, C.-S. Lin, X.-M. Wang, L. Ding, C.-L. Cui, S.-F. Liu, H. Y. Lu, *Chem. Commun.*, 2010, **46**, 3765–3767.
32 E. Karakuş, M. Üçüncü, M. Emrullahoğlu, *Chem. Commun.*, 2014, **50**, 1119–1121.
33 Y. S. Kim, J. J. Lee, Y. W. Choi, G. R. You, L. Nguyen, I. Noh, C. Kim, *Dyes Pigm.*, 2016, **129**, 43–53.
34 X. Zhou, P. Li, Z. Shi, X. Tang, C. Chen, W. Liu, *Inorg. Chem.*, 2012, **51**, 9226−9231.
35 A. Kuwar, R. Patil, A. Singh, S. K. Sahoo, J. Marek, N. Singh, *J. Mater. Chem. C*, 2015, **3**, 453–460.
36 H. Y. Jeong, S. Y. Lee, J. Han, M. H. Lim, C. Kim, *Tetrahedron*, 2017, **73**, 2690–2697.
37 T. Q. Liu, X. J. Wan, Y. W. Yao, *Sens. Actuators B*, 2018, **254**, 1094–1100.
38 L. Wang, W. Qin, X. Tang, W. Dou, W. Liu, *J. Phys. Chem. A*, 2011, **115**, 1609–1616.
39 L. McDonald, J. Wang, N. Alexander, H. Li, T. Liu, Y. Pang, *J. Phys. Chem. B*, 2016, **120**, 766−772.
40 S. Goswami, S. Das, K. Aich, D. Sarkar, T. K. Mondal, C. K. Quah, H.-K. Fun, *Dalton Trans.*, 2013, **42**, 15113–15119.
41 Frisch MJ. Gaussian 09, Revision A.1, Gaussian Incorp, Wallingford, CT 2009.
42 X. Geng, X. Mo, L. Fan,, A. Yin, J. Fang, *J. Mater. Chem.*, 2012, **22**, 25130–25139.
43 I. H. Hwang, Y. W. Choi, K. B. Kim, G. J. Park, J. J. Lee, L. Nguyen, I. Noh, C. Kim, *New J. Chem.*, 2016, **40**, 171–178.
44 R. Rahier, A. Noiriel, A. Abousalham, *Anal. Chem.*, 2016, **88**, 666−674.
45 H.-L. Lu, W.-K. Wang, X.-X. Tan, X.-F. Luo, M.-L. Zhang, M. Zhang, S.-Q. Zang, *Dalton Trans.*, 2016, **45**, 8174–8181.

View Article Online
DOI: 10.1039/C8TB01743C

46 S. J. Malthus, S. A. Cameron, S. Brooker, *Inorg. Chem.*, 2018, **57**, 2480−2488.
47 H. J. Jang, J. H. Kang, M. Lee, M. H. Lim, C. Kim, *Ind. Eng. Chem. Res.*, 2018, **57**, 54−62.
48 S. Sinha, B. Chowdhury, P. Ghosh, *Inorg. Chem.*, 2016, **55**, 9212−9220.
49 D. Brodbeck, F. Broghammer, J. Meisner, J. Klepp, D. Garnier, W. Frey, J. Kästner, R. Peters, *Angew. Chem. Int. Ed.*, 2017, **56**, 4056–4060.
50 J. Zhang, T. E. Brutus, J. Cheng, X. Meng, *J. Environ. Sci*., 2017, **57**, 190–195.
51 L. Xu, M.-L. He, H.-B. Yang, X. H. Qian, *Dalton Trans.*, 2013, **42**, 8218–8222.
52 S. Dong, W. Shi, J. Zhang, S. Bi, *ACS Earth Space Chem*., 2018, **2**, 269−277.
53 J.-T. Hou, W. X. Ren, K. Li, J. Seo, A. Sharma, X.-Q. Yu, J. S. Kim, *Chem. Soc. Rev*., 2017, **46**, 2076–2090.
54 D. C. Harris, Quantitative chemical analysis, eighth ed, New York: Freeman, 2010, p: 242.
55 World Health Organization, Guidelines for drinking-water quality, 4th ed.; World Health Organization: Geneva, 2011, 1, p: 459.
56 H. A. Benesi, J. H. Hildebrand, *J. Am. Chem. Soc.*, 1949, **71**, 2703–2707.
57 K. C. Sham, C. S. Lee, K. Y. Chan, S. M. Yiu, W. T. Wong, H. L. Kwong, *Polyhedron*, 2011, **30**, 1149–1156.
58 S. Goswami, S. Paul, A. Manna, *RSC Adv*., 2013, **3**, 25079–25085.
59 A. Ghosh, D. Das, *Dalton Trans.*, 2015, **44**, 11797–11804.
60 A. J. Qin, B. Z. Tang, Aggregation-Induced Emission: Fundamentals, Chapter 7th, John-Wiley & Sons, Ltd., 2014, p:157.
61 X. Y. Shen, Y. J. Wang, E. Zhao, W. Z. Yuan, Y. Liu, P. Lu, A. J. Qin, Y. Ma, J. Zhi Sun, B. Z. Tang, *J. Phys. Chem. C*, 2013, **117**, 7334−7347.
62 T. Soboleva, H. J. Esquer, A. D. Benninghoff, L. M. Berreau, *J. Am. Chem. Soc.*, 2017, **139**, 9435−9438.
63 S. Erbas-Cakmak, S. Kolemen, A. C. Sedgwick, T. Gunnlaugsson, T. D. James, J. Yoon, E. U. Akkaya, *Chem. Soc. Rev*., 2018, **47**, 2228–2248.
64 X. Zheng, R. Fan, K. Xing, A Wang, X. Du, P. Wang, Y. Yang, *J. Mater. Chem. C*, 2018, **6**, 6229–6239.